Supplement of

Impacts of synoptic circulation types on nocturnal ozone increase in the North China Plain: Meteorological drivers and formation mechanisms

Huanpeng Wang et al.

Correspondence to: Liya Fan (fanly@scut.edu.cn)

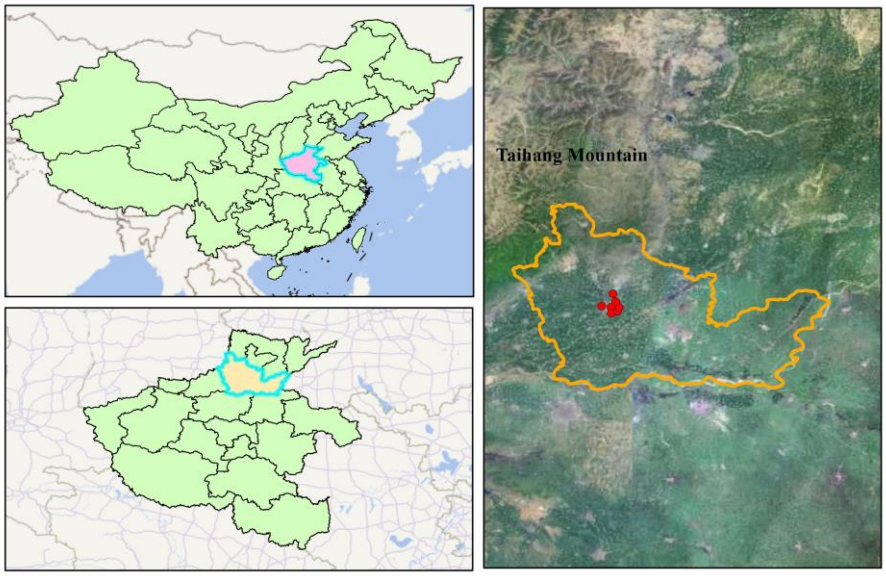

Figure S1: Location of Xinxiang and national air quality monitoring stations in Xinxiang (There are seven national air quality monitoring stations (Development Zone (KF), Municipal Government (ZF), Environmental Protection East Hospital (DY), Environmental Protection West Court (XY), Administrative Service Center (FW), Municipal Party School (DX), Henan Normal University (SD)). Based on data completeness criteria from 2021 to 2023, four stations (KF, DY, XY, and DX) were selected for analysis).

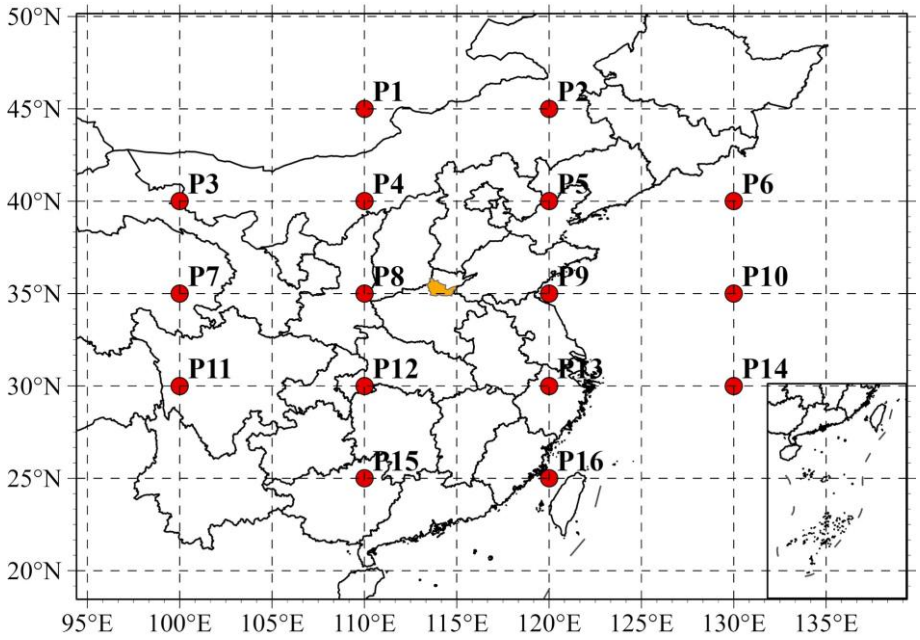

Figure S2: Lamb-Jenkinson synoptic circulation classification grid diagram (P1-P16 are the 16 grid points selected, and the orange area is Xinxiang).

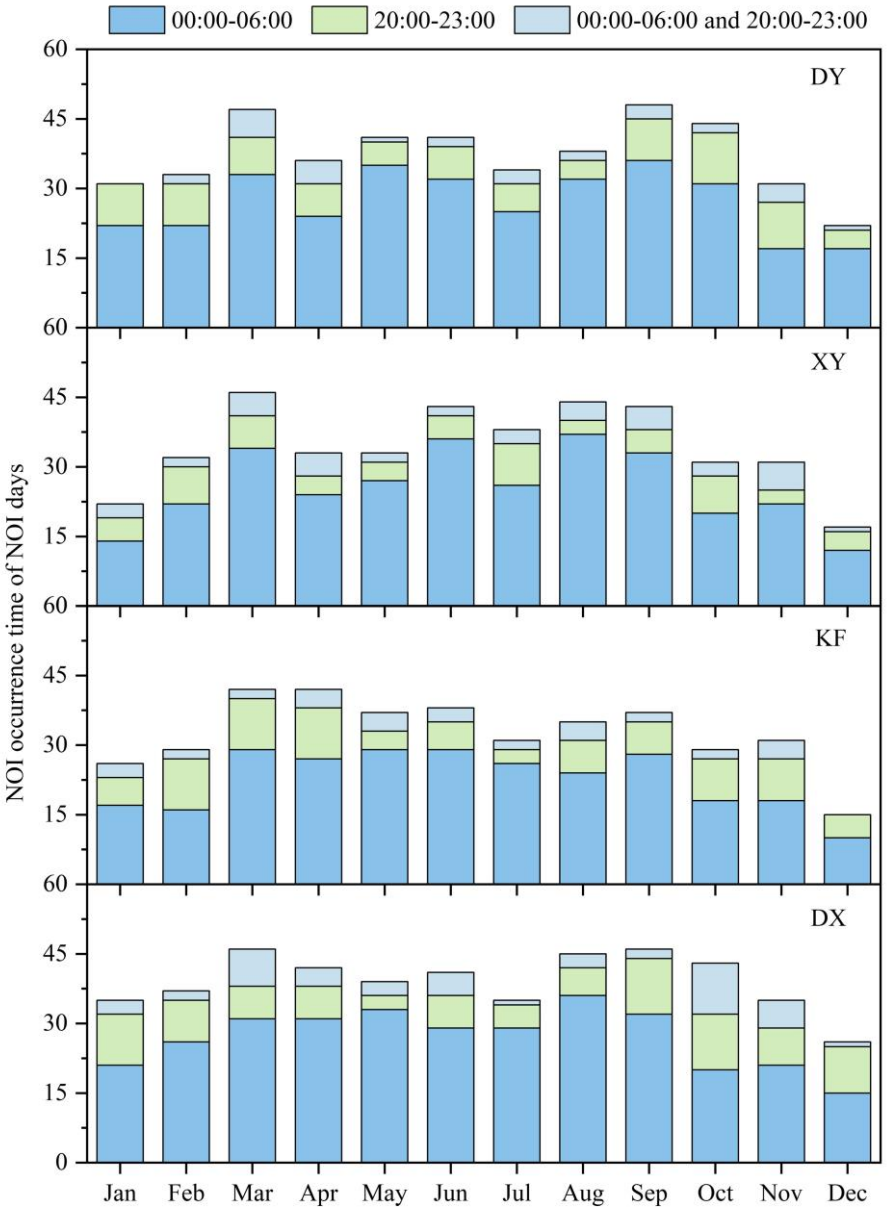

Figure S3: Monthly variation of NOI occurrence time at national monitoring stations in Xinxiang, 2021-2023.

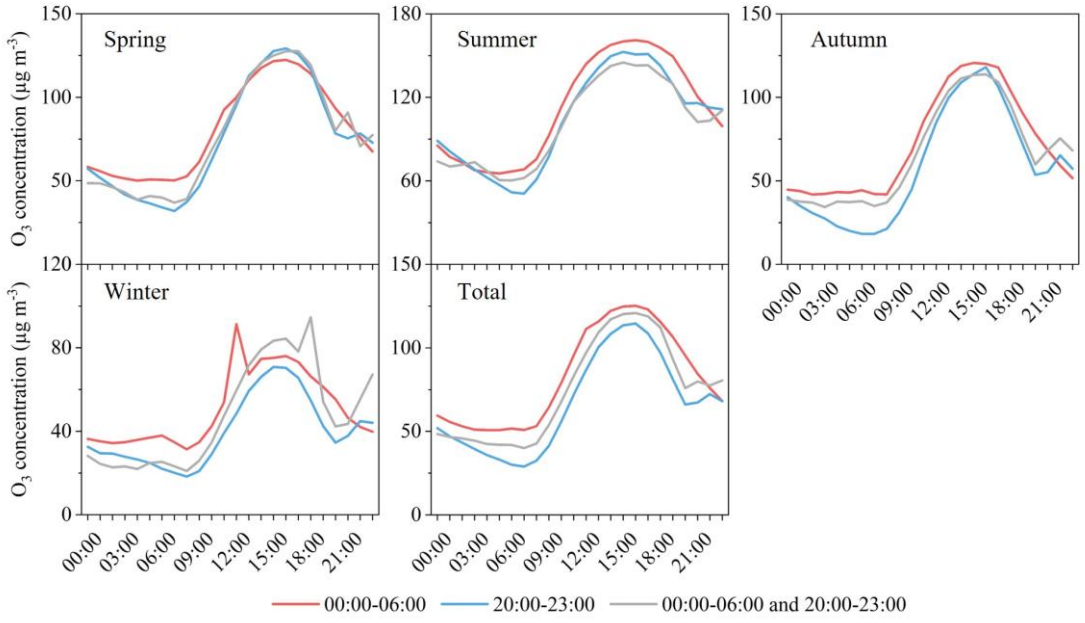

Figure S4: O_3 diurnal variations of NOI days under different NOI occurrence time in different seasons.

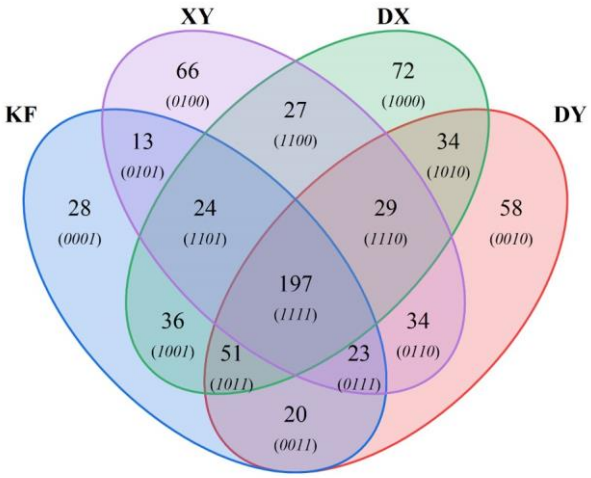

Figure S5: Overlapping occurrences of NOI days outbreak dates at national monitoring stations in Xinxiang, 2021-2023.

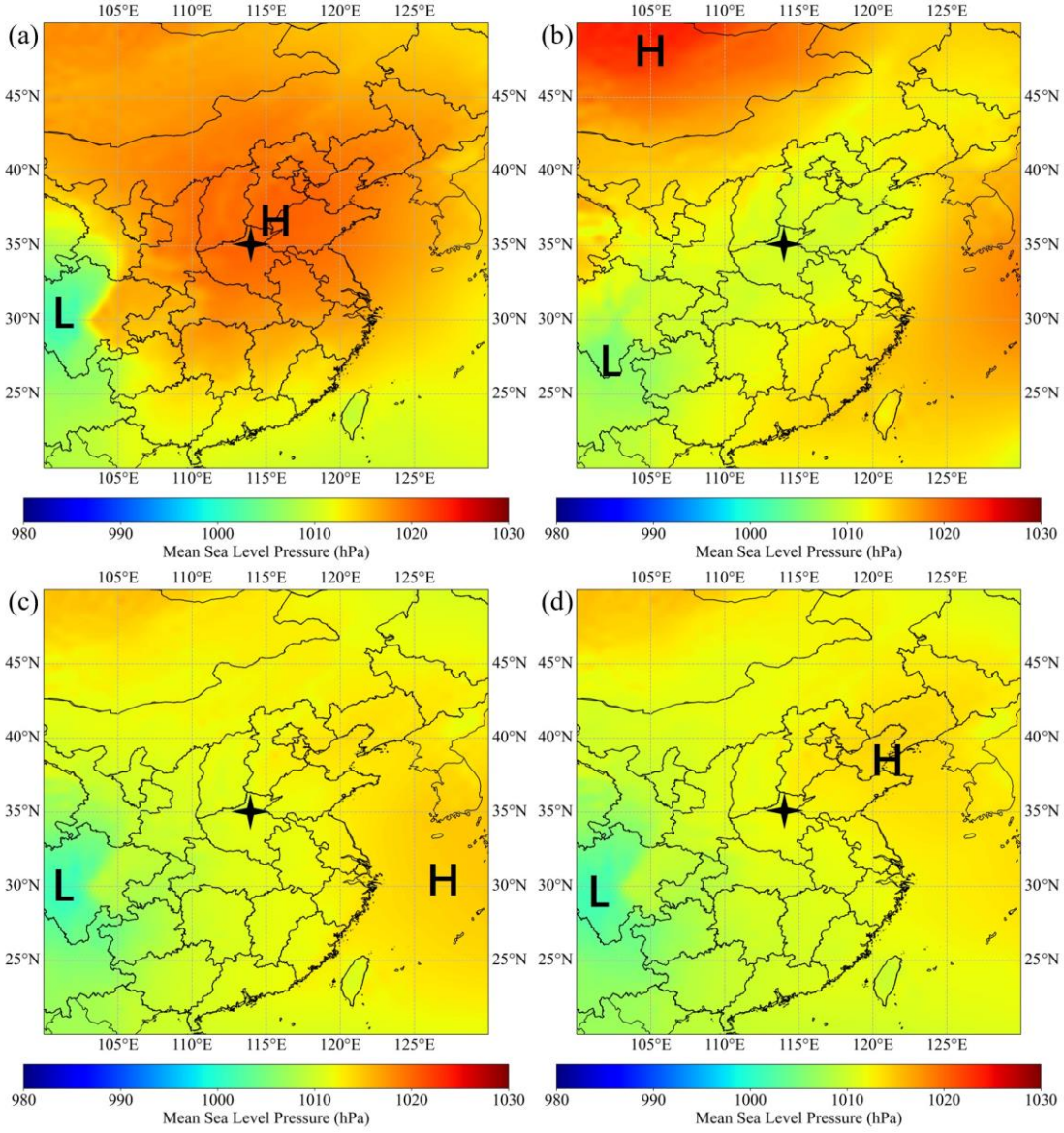

Figure S6: Mean SLP under different weather types for representative NOI days: (a) vorticity type A, (b) vorticity type C, (c) direction types, (d) hybrid types (asterisk indicates the location of Xinxiang; "H" and "L" stand for high-pressure and low-pressure, respectively).

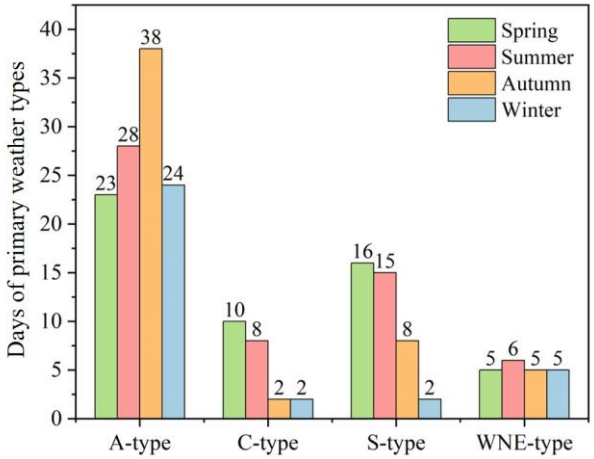

Figure S7: Seasonal variations of the four primary weather types in Xinxiang.

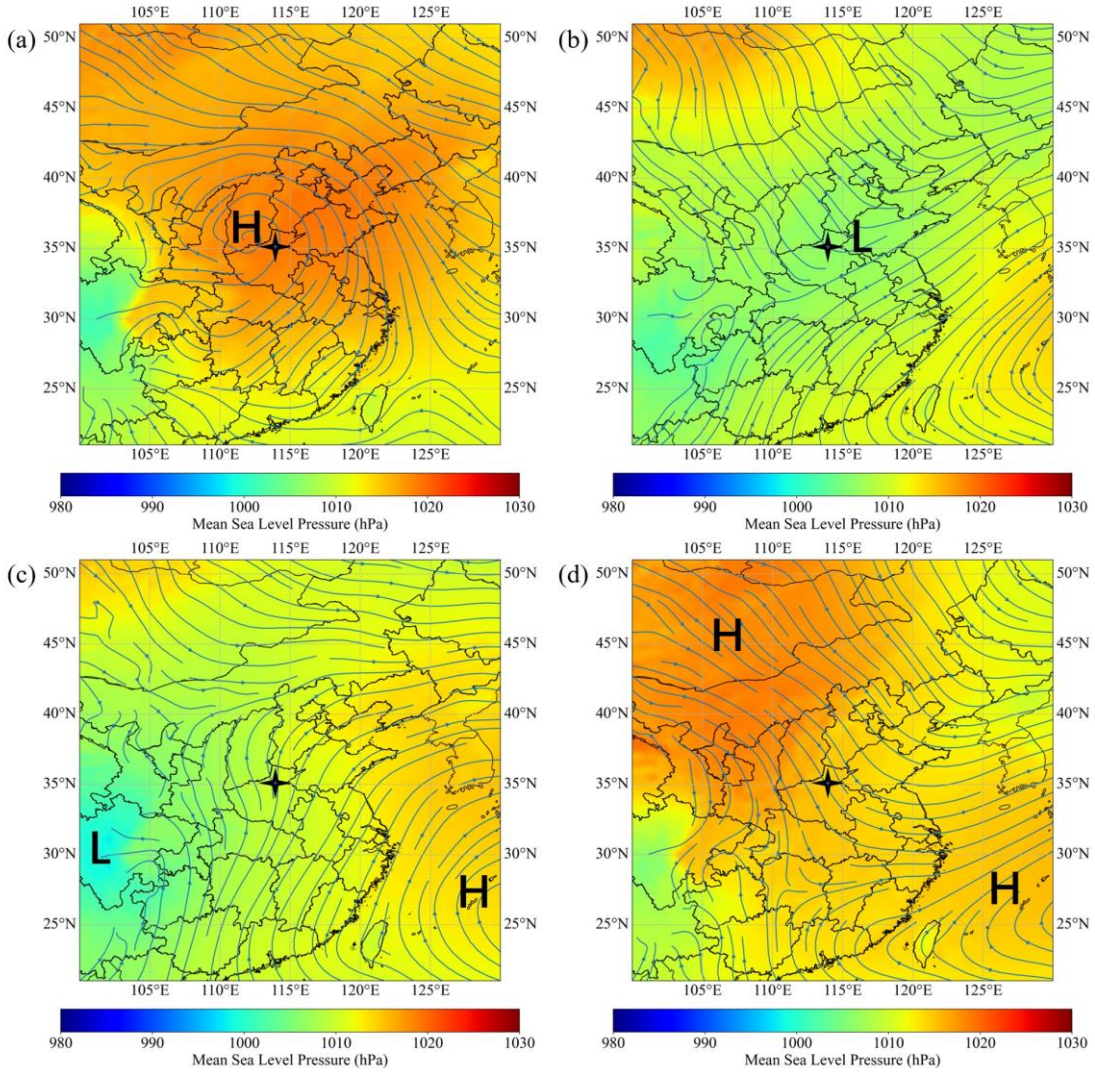

Figure S8: Spatial distribution of SLP under different weather types: (a) A-type, (b) C-type, (c) S-type, (d) WNE-type (asterisk indicates the location of Xinxiang; "H" and "L" stand for high-pressure and low-pressure, respectively).

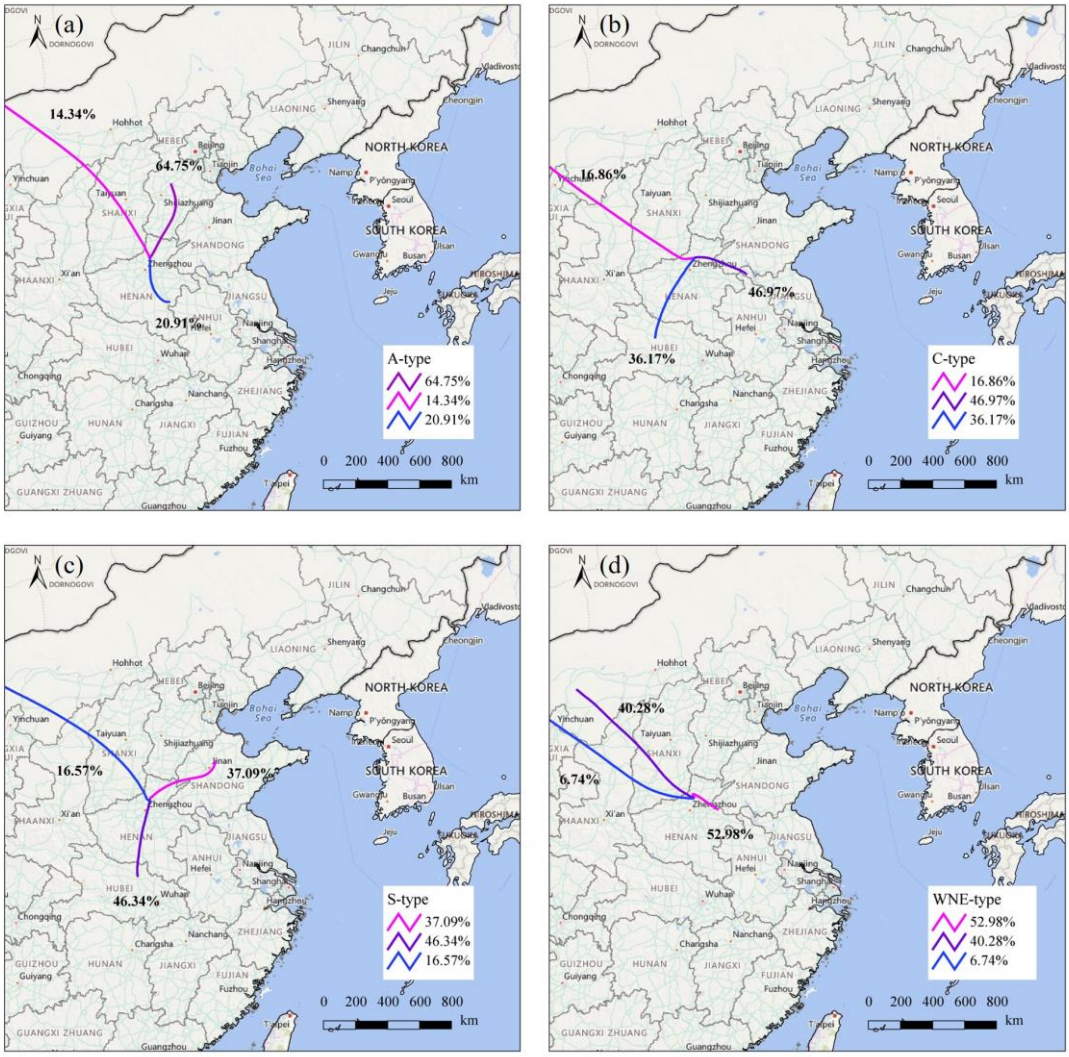

Figure S9: Clustered backward trajectories under different weather types: (a) A-type, (b) C-type, (c) S-type, (d) WNE-type.

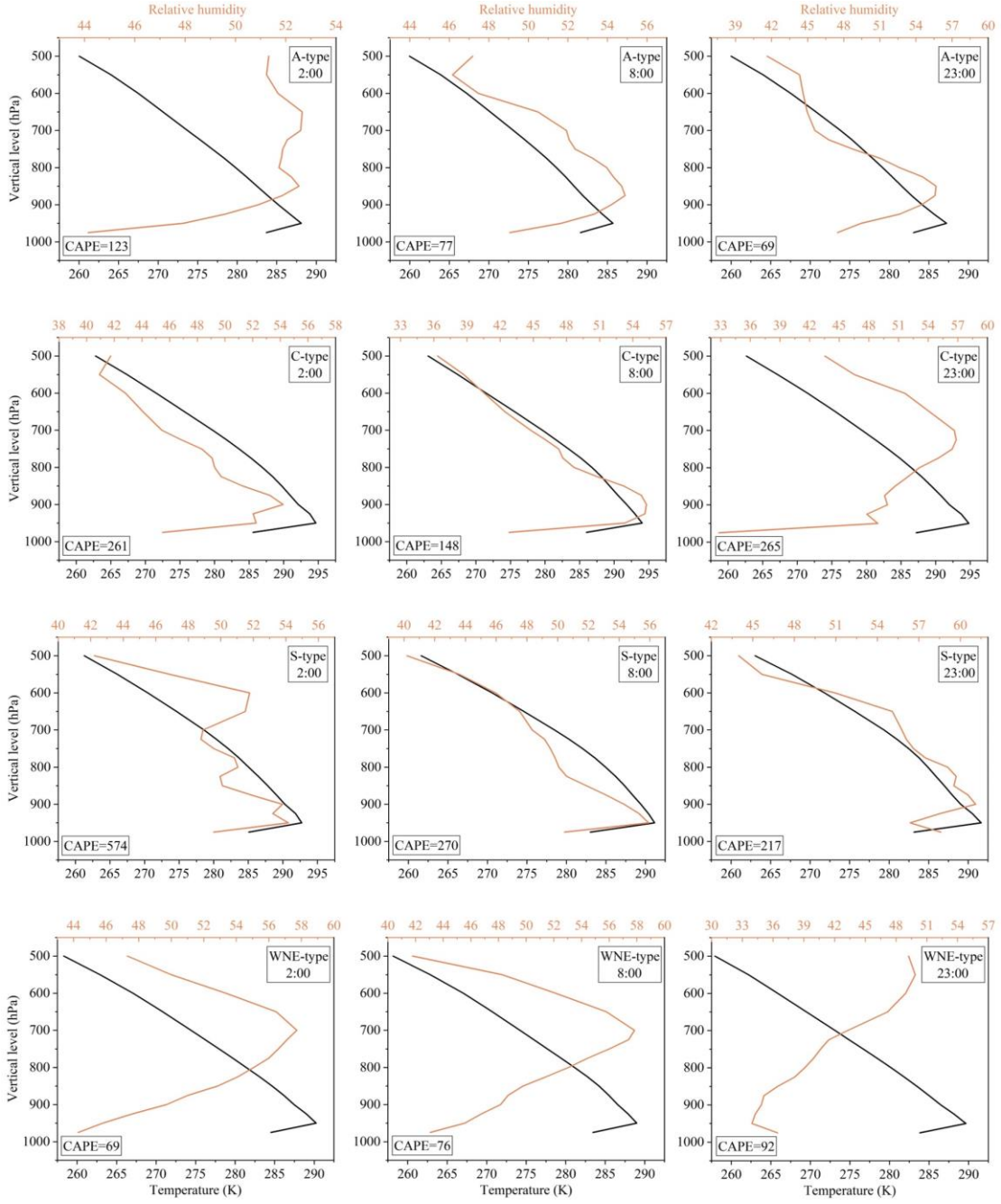

Figure S10: Vertical profiles of temperature and relative humidity of Xinxiang under the four weather types.

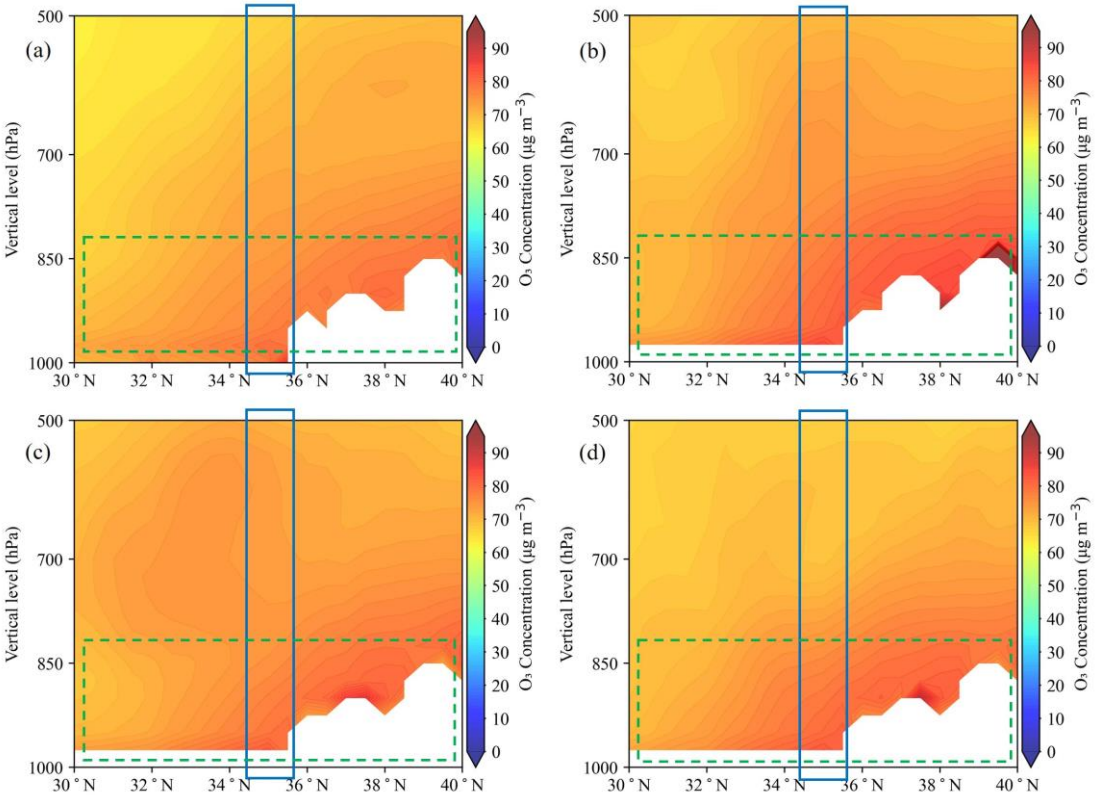

Figure S11: Vertical profiles of average O_3 concentration under different weather types: (a) A-type, (b) C-type, (c) S-type, (d) WNE-type (blue rectangles indicate the region of Xinxiang; green rectangles (dashed lines) indicate regions with high O_3 concentration).

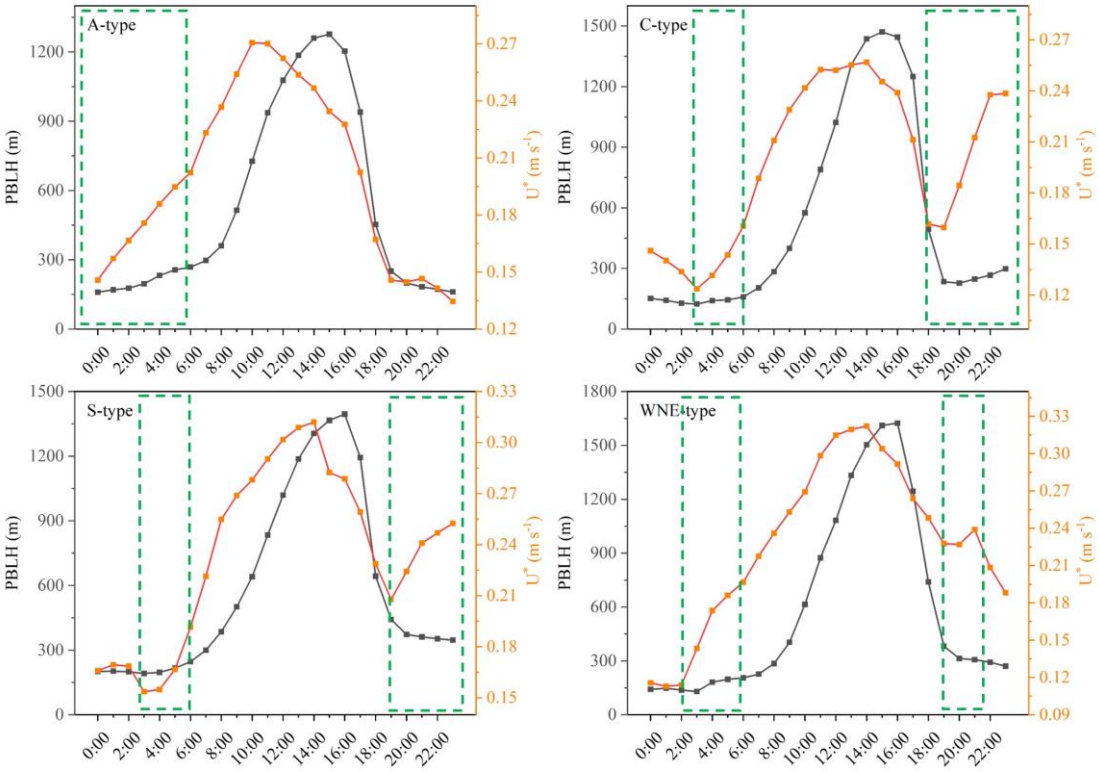

Figure S12: Diurnal variations of planetary boundary layer height (PBLH) and friction velocity (U^*) in Xinxiang under four weather types (green dashed lines rectangles indicate the fluctuations of PBLH or U^* during the night.).

Table S1. Weather classification results of representative NOI days in Xinxiang, 2021-2023.

	Weather type	2021	2022	2023	Total	Percentage
Vorticity types	A	25	27	30	82	46.19 %
	C	2	2	5	9	
Directional types	S	9	7	2	18	31.47 %
	SE	6	4	3	13	
	SW	2	4	4	10	
	W	3	2	2	7	
	NW	0	0	1	1	
	N	0	1	2	3	
	NE	1	2	2	5	
	E	1	2	2	5	
Hyrid types	AE	5	1	2	8	22.34 %
	AN	1	0	1	2	
	ANE	1	0	0	1	
	ANW	1	0	0	1	
	AS	2	4	4	10	
	ASE	5	0	3	8	
	AW	1	0	0	1	
	CE	1	2	1	4	
	CN	0	1	0	1	
	CS	0	2	0	2	
	CSE	0	1	0	1	
	CSW	2	1	0	3	
	CW	0	1	1	2	

Table S2. Average temperature, relative humidity, wind speed, wind direction and precipitation observed on the ground in Xinxiang under four weather types.

Weather Type	Temperature (℃)	Relative humility (%)	Wind speed (m s^{-1})	Wind direction (°)	Precipitation (mm h^{-1})
A-type	15.53	64.31	2.75	127.48	0.19
C-type	19.30	72.43	2.24	139.69	0.49
S-type	17.58	70.50	2.53	136.77	0.24
WNE-type	16.48	59.20	2.78	171.98	0.13

Table S3: Average temperature, relative humidity, wind speed, wind direction and precipitation observed on the ground in Xinxiang under four weather types in different seasons.

Weather Type	Season	Temperature (℃)	Relative humility (%)	Wind speed (m s^{-1})	Wind direction (°)	Precipitation (mm h^{-1})
A-type	Spring	15.65	59.85	3.09	116.30	0.143
	Summer	23.63	73.73	2.00	134.28	0.522
	Autumn	15.71	65.46	2.83	120.70	0.063
	Winter	5.98	55.99	3.15	140.76	0.026
C-type	Spring	20.70	72.77	2.55	130.52	0.325
	Summer	23.26	75.39	1.95	126.68	0.944
	Autumn	6.86	73.77	1.28	173.90	0
	Winter	8.79	56.75	2.71	209.06	0
S-type	Spring	16.68	68.25	2.97	137.74	0.103
	Summer	24.12	75.87	1.93	140.08	0.325
	Autumn	10.86	71.33	2.52	133.04	0.249
	Winter	4.15	46.77	3.55	119.81	0.608
WNE-type	Spring	16.32	55.45	3.27	161.79	0.002
	Summer	23.67	64.95	2.09	165.61	0.117
	Autumn	14.28	66.47	2.73	139.29	0.385
	Winter	10.65	48.76	3.12	223.50	0.038

Text S1: Concentration weighted trajectory (CWT) analysis.

The concentration weighted trajectory (CWT) analysis method quantifies the distribution of pollutant concentrations by calculating the weighted average concentration of air mass trajectories, providing a visual representation of pollution levels (Shi et al., 2024; Zhang et al., 2024). The calculation formula is as follows:

$$C_{ij} = \frac{\sum_{l=1}^{M} C_l \cdot \tau_{ijl}}{\sum_{l=1}^{M} \tau_{ijl}} \quad (1)$$

where C_{ij} represents the average weighted concentration on grid (i,j), C_l is the pollutant concentration corresponding to the trajectory passing through grid (i,j), and τ_{ijl} is the residence time of the trajectory in the grid. To reduce uncertainty, a weighting coefficient is introduced, and the corrected value is denoted as WCWT (Zhang et al., 2024; Wang et al., 2024). The calculation formula is as follows:

$$WCWT = C_{ij} \times W_{ij} \quad (2)$$

where W_{ij} is the weighting coefficient with specific values (Wang et al., 2024):

$$W_{ij} = \begin{cases} 1.00, & n > 80 \\ 0.70, & 20 < n \leq 80 \\ 0.42, & 10 < n \leq 20 \\ 0.05, & n \leq 10 \end{cases} \quad (3)$$

where n represents the number of trajectories in the grid.

References

Shi, J., Wu, X., Han, X., Zhong, Y., Wang, Z., and Ning, P.: Characterization and sources of carbonaceous aerosols in southwest plateau of China: Effects of biomass burning and low oxygen concentration, Atmos. Environ., 318, 120250, https://doi.org/10.1016/j.atmosenv.2023.120250, 2024.

Wang, G., Liu, X., Kong, F., Zhu, Z., Yan, P., Gao, W., and Zhao, N.: Characteristics of fine particulate matter in Linyi during the 24th Olympic winter Games: An insight into the components, sources, transport pathways, and source distribution, Atmos. Pollut. Res., 15, 102034, https://doi.org/10.1016/j.apr.2023.102034, 2024.

Zhang, L., Yang, L., Kashiwakura, K., Zhao, L., Chen, L., Han, C., Nagao, S., and Tang, N.: Autumn and spring observations of $PM_{2.5}$-bound polycyclic aromatic hydrocarbons and nitro-polycyclic aromatic hydrocarbons in China and Japan, Environ. Pollut., 343, 123139, https://doi.org/10.1016/j.envpol.2023.123139, 2024.